

CERIA-MANGANESE OXIDE CATALYST ACTIVITY - OZONE DECOMPOSITION AND DISCOLORATION OF MALACHITE GREEN DYE

Katerina Zaharieva¹, Petya Karakashkova², Daniela Stoyanova³, Silvia Dimova⁴,
Ognian Dimitrov⁵, Irina Stambolova³

¹Institute of Mineralogy and Crystallography "Acad. I. Kostov"
Bulgarian Academy of Sciences, "Acad. G. Bonchev" St.
Block 107, 1113 Sofia, Bulgaria

Received 27 January 2023
Accepted 25 February 2023

²Institute of Catalysis, Bulgarian Academy of Sciences
"Acad. G. Bonchev" St., Block 11, 1113 Sofia, Bulgaria

³Institute of General and Inorganic Chemistry
Bulgarian Academy of Sciences, "Acad. G. Bonchev" St., Block 11
1113 Sofia, Bulgaria

⁴Institute of Polymers, Bulgarian Academy of Sciences
"Acad. G. Bonchev" St., Block 103A, 1113 Sofia, Bulgaria

⁵Institute of Electrochemistry and Energy Systems
"Academician Evgeni Budevski"
Bulgarian Academy of Sciences, "Acad. G. Bonchev" St.
Block 10, 1113, Sofia, Bulgaria
E-mail: zaharieva@imc.bas.bg

ABSTRACT

In the present study CeO_2 - Mn_2O_3 oxides catalyst was prepared using Pluronic-assisted co-precipitation. The phase composition, structure, morphology, specific surface area and textural characteristics of synthesized material were investigated by X-ray diffraction analysis, Fourier-transform infrared spectroscopy, Scanning electron microscopy, nitrogen adsorption-desorption isotherm and BET method. The X-ray diffraction analysis established the presence of CeO_2 and Mn_2O_3 phases. The synthesized mesoporous CeO_2 - Mn_2O_3 oxides have specific surface area ($S_{BET} = 102 \text{ m}^2 \text{ g}^{-1}$), total pore volume ($0.47 \text{ cm}^3 \text{ g}^{-1}$) and average pore diameter (18 nm). The CeO_2 - Mn_2O_3 oxides catalyst was tested in two reactions - ozone decomposition and photocatalytic discoloration of Malachite Green (MG) dye as model pollutant under UV light. The ozone conversion over CeO_2 - Mn_2O_3 oxides catalyst was reached about 73 %. After that, the ozonated catalyst was tested in the photocatalytic reaction for removal of MG dye and its UV- light photocatalytic activity was compared with freshly prepared CeO_2 - Mn_2O_3 photocatalyst. The higher degree of discoloration of MG dye (62 %) was achieved in the presence of ozone treated CeO_2 - Mn_2O_3 oxides photocatalyst.

Keywords: catalyst, ozone decomposition, Malachite Green dye.

INTRODUCTION

Ozone (O_3) is a powerful oxidant that adversely affects human health and ecosystems. High-levels of ozone can cause cardiovascular and respiratory dysfunction and increase mortality [1]. The ozone decomposition is technologically important process for environmental protection. The ozone levels in airplane cabins, offices, submarine, sterilization and deodorization units and discharges from wastewater treatment have to be reduced [2]. Catalytic decomposition

is the most promising method for O_3 removal because it is safe, effective and economical [1, 3]. Among the catalysts, applied for ozone decomposition the transition metal oxides have been widely studied due to their redox activity, variable valence states and good stability. The researchers have proved that the oxides of Mn, Co, Ce, Ni, Cr, Ag, Cu, Fe and Mo exhibit high catalytic activity in the ozone decomposition reaction [4 - 11]. Among the three investigated manganese dioxides (α , β - and γ - MnO_2), obtained by hydrothermal method, α - MnO_2 exhibited the highest catalytic activity [6]. Another

research group have prepared catalyst based on ϵ - MnO_2 which has demonstrated high ozone conversion (91.3 %) [7]. Various oxide catalysts such as: CeO_2 [12, 13], cerium-rare earth mixed oxides [13], Ce-MnO_x [14], copper, manganese and copper-manganese oxides on Al support [15], manganese oxide supported on ZrO_2 and TiO_2 [16] have been also investigated.

Many industries used dyes (textile dyeing, paper making, food processing, cosmetics, paints etc.) and pollute wastewaters having an adverse effect on ecosystems and human health [17].

The widely used Malachite Green dye possesses toxic properties which cause mutagenesis, teratogenesis, carcinogenesis and respiratory toxicity. The removal of MG from wastewater before release in the environment is very important and necessary action [18]. For this reason, we choose Malachite Green dye as model pollutant in our investigations.

Photocatalysis is a perspective eco-friendly method for the water purification from various organic contaminants [19]. Cerium dioxide catalysts prepared by green synthesis revealed high photocatalytic activity for model dye degradation [20, 21]. A Ca-doped ceria nanoparticles photocatalyst have been prepared by co-precipitation technique using ammonium oxalate as a precipitating agent. Ca-doped ceria catalyst degraded 93 % of MG dye after 90 min UV irradiation. [22]. The hierarchical Mn_2O_3 nanomaterials have exhibited also enhanced photocatalytic ability towards degradation of Methylene Blue dye [23, 24]. Mesoporous ceria has been prepared using soft template technique using Pluronic P123 by [25, 26]. B. Deljoo et al. have been obtained mesoporous manganese oxides (mixture of Mn_3O_4 and Mn_5O_8) using the UCT inverse micelle templating method with Pluronic surfactants [27].

The main goals of the present work are:

- (i) synthesis of non-treated and ozone treated CeO_2 - Mn_2O_3 catalysts using Pluronic-assisted co-precipitation;
- (ii) comparison of their catalytic effectiveness for two ecologically important reactions - ozone decomposition and UV- initiated discoloration of Malachite Green dye.

EXPERIMENTAL

Synthesis of CeO_2 - Mn_2O_3 catalyst

The CeO_2 - Mn_2O_3 catalyst was prepared using 0.09 M aqueous solutions of $\text{Ce}(\text{NO}_3)_3 \cdot 6\text{H}_2\text{O}$ (Alfa Aesar)

and $\text{Mn}(\text{NO}_3)_2 \cdot 4\text{H}_2\text{O}$ (Alfa Aesar) mixed in ratio 1:1 and stirred for 10 minutes. Tri-block copolymer Pluronic P123 (Sigma-Aldrich, Mw = 5800) was dissolved in distilled water (5 g in 50 mL) under stirring for 1 hour and added to the above prepared mixture of metal precursors. This final solution was stirred for 10 minutes. The precipitant 2 M NaOH (Valerus Co.) was added drop by drop in the final mixture until pH reached 11 under continuous stirring for one hour. The precipitate was filtered, washed with distilled water several times and dried at 35°C. The dried material was calcined at 500°C for 4 hours in air.

Characterizations

The physicochemical characterization of the prepared catalyst was performed by X-ray diffraction (XRD) analysis, Fourier-transform infrared (FT-IR) spectroscopy, Scanning electron microscopy (SEM) and BET method. The XRD analysis was carried out on a Bruker D2 Phaser diffractometer within the range of 2θ values between 20° and 85° using Cu K α radiation ($\lambda = 0.154056$ nm) at 40 kV. JCPDS database (Powder Diffraction Files, Joint Committee on Powder Diffraction Standards, Philadelphia PA, USA) was used to establish the presence of phases. FT-IR spectra were performed on a Fourier infrared spectrometer Bruker-Vector 22 in the 400 cm^{-1} - 4000 cm^{-1} range and using KBr pellets. The morphology of the prepared material was studied using scanning electron microscope (apparatus JEOL JEM-200CX) at accelerating voltage 80 keV. The express BET method was applied to measure the specific surface area, based on low-temperature adsorption of nitrogen. The relative error of the method is about 8 %. The specific surface area and the pore size distribution measurements were performed on an automated apparatus NOVA Win-CFR Quantachrom-Gas Sorption System. The surface area was calculated using the BET equation, whereupon the pore size distribution and the average pore diameter were evaluated by the DFT method assuming a cylindrical model of the pores. The total pore volume was estimated in accordance with the rule of Gurvich at relative pressure of 0.96.

Ozone decomposition study

The ozone conversion has been studied by monitoring of change on the ozone concentration. The experiment was carried out in tubular glass reactor filled with

0.15 g catalyst. Ozone was obtained by passing dried oxygen (99.99 %) through a 4 - 9 kV discharge in a self-made design, tubular type of ozone generator. An ozone-oxygen mixture with inlet ozone concentration within 10 000 ppm was passed through the reactor at a flow rate of about 6.0 l h⁻¹ at ambient temperature. The ozone concentration at the reactor inlet and outlet were measured spectrophotometrically by BMT model 964 ozone analyzer.

Photocatalytic tests

Malachite Green (MG) was used as model contaminant (5 ppm aqueous solution of dye). The photocatalytic experiments were performed under UV-A illumination (18 W) in semi-batch slurry reactor using 0.15 g photocatalyst suspended previously in 150 ml of dye solution under constant stirring and air flowing. In order to reach adsorption-desorption equilibrium state the studied systems were left in the dark for about 30 min before switching on the irradiation for 2 hours. The powder was separated from the aliquot solution by centrifugation. After that the change of absorbance during the photocatalytic tests was monitored by UV-Vis absorbance spectrophotometer UV-1600PC in the wavelength range from 200 nm to 800 nm ($\lambda_{\max} = 615$ nm).

RESULTS AND DISCUSSION

The recorded X-ray diffraction pattern of synthesized CeO₂-Mn₂O₃ material is presented on Fig. 1. The presented diffractogram is characteristic for the presence of CeO₂ (PDF- 00-004-0593) and Mn₂O₃ (PDF-00-041-1442) phases. The pattern reveals that the material possesses low degree of crystallization. The average crystallite size (*D*), lattice strain (ϵ) and unite cell parameter (*a*) of investigated CeO₂ and Mn₂O₃ phases are calculated by PowderCell 2.4 program [28] and using Williamson–Hall equation [29]:

$$\beta \cos\theta = 0.9 \lambda/D + 4\epsilon \sin\theta \quad (1)$$

where ϵ is the value of internal strain, β is the full-width half-maximum (FWHM) of diffraction, θ is the Bragg's angle, λ is the wavelength of X-ray beam used and *D* is the average crystallite size of the phase under study.

The evaluated parameters are presented in Table 1. The

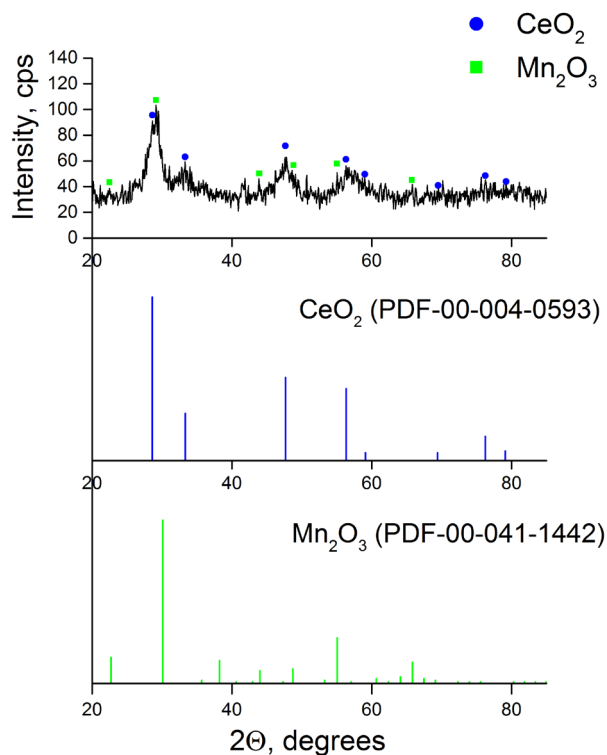


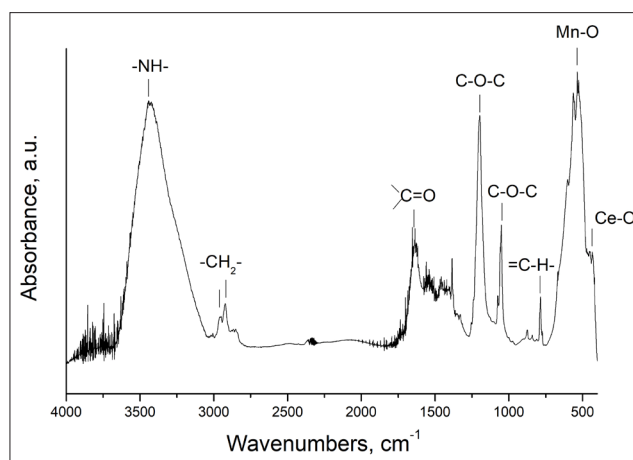
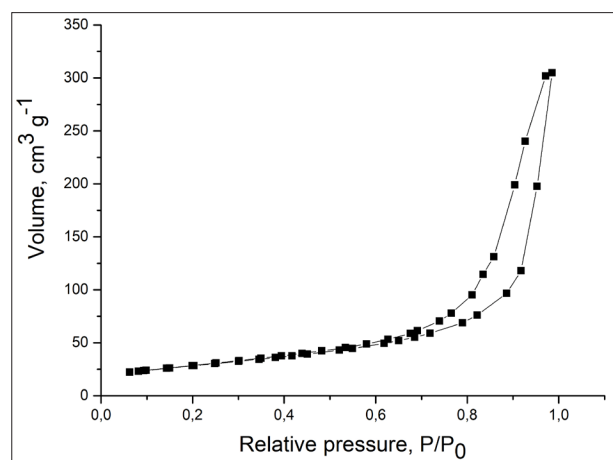
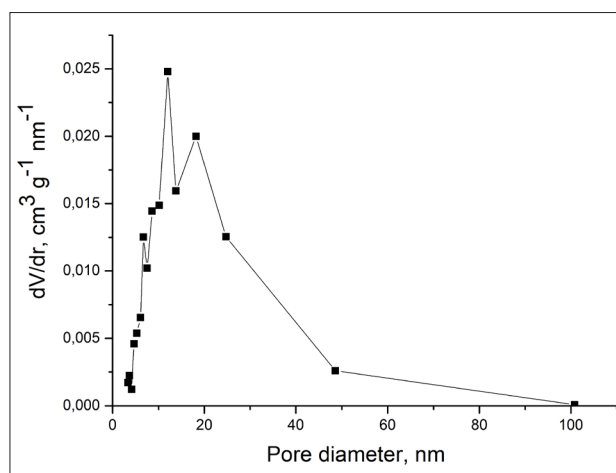
Fig. 1. XRD pattern of CeO₂-Mn₂O₃ catalyst.

Table 1. Calculated values of mean crystallite size (*D*), lattice strain (ϵ) and unite cell parameter (*a*) of CeO₂ and Mn₂O₃ phases in prepared material.

Sample	<i>D</i> (nm)	$\epsilon \times 10^{-3}$ (a.u.)	<i>a</i> , (Å)
CeO ₂	10	4.3	5.41
Mn ₂ O ₃	29.5	0.6	9.41

smaller average crystallite size is established for CeO₂ phase (10 nm) than that of the Mn₂O₃ (29.5 nm) probably due to the inhibition the growth of ceria crystallites by Mn particles [30].

The FT-IR spectrum of synthesized material is displayed on Fig. 2. The absorption peak at 450 cm⁻¹ is associated with the CeO₂ stretching vibration [31]. The signal at 530 cm⁻¹ corresponds to $\nu_{\text{Mn-O}}$ of Mn₂O₃ [32]. The peaks in the region 2975 cm⁻¹ - 2875 cm⁻¹ are due to symmetric and asymmetric stretching vibrations of the aliphatic groups (-CH₂-)_n of the Pluronic P123. The vibrations observed at about 3439 cm⁻¹ are characteristics

Fig. 2. FT-IR spectrum of CeO₂-Mn₂O₃ catalyst.Fig. 3. The nitrogen adsorption-desorption isotherm of CeO₂-Mn₂O₃ catalyst.Fig. 4. Pore size distribution of CeO₂-Mn₂O₃ catalyst.

for the presence of the NH group. The peak positioned at 1700 cm⁻¹ is indication for CO group. The bands observed at about 1150 cm⁻¹ - 1400 cm⁻¹ and 785 cm⁻¹ are assigned to stretching vibration C-O-C and bending vibration =C-H- of Pluronic P123, respectively [33, 34]. The presence of absorption bands of Pluronic P123 in the FT-IR spectrum of the CeO₂-Mn₂O₃ catalyst after calcination procedure could be assigned to the “delayed” decomposition of the polymer template, which is due to the interaction with mixed metal oxides [35 - 37].

The isotherm presented in Fig. 3 can be classified as V type according to the IUPAC nomenclature. The hysteresis loop according to the same nomenclature is of the H3 type, which closes at a relative pressure p/p_0 of about 0.4 - 0.5. This shape of the hysteresis is an indication of the biporous structure of the sample. This suggests the presence of toroidal pores, and perhaps also

the presence of bottle-shaped pores.

The pore size distribution of the prepared CeO₂-Mn₂O₃ oxides sample shown in Fig. 4 follows the bimodal model. A small relative share of fine mesopores, the size of which is in the range of 5 nm - 15 nm, is observed. Mesopores in the 20 nm - 50 nm range have a larger relative part. The synthesized CeO₂-Mn₂O₃ catalyst possesses specific surface area ($S_{\text{BET}} = 102 \text{ m}^2 \text{ g}^{-1}$), total pore volume ($V_t = 0.47 \text{ cm}^3 \text{ g}^{-1}$) and average pore diameter ($D_{\text{av}} = 18 \text{ nm}$).

The morphology of synthesized CeO₂-Mn₂O₃ catalyst is investigated using Scanning electron microscopy (SEM). The SEM images at different magnifications reveal the presence of rough agglomerates with different sizes (Fig. 5). It is known that the agglomeration is a more energetically stable configuration and allows growth of the crystallites [38]. The all results, obtained from XRD analysis, FT-IR spectroscopy, SEM, nitrogen adsorption-desorption isotherm and BET method about phase composition, structure, morphology and textural characteristics of synthesized CeO₂-Mn₂O₃ catalyst are in agreement.

The catalytic ability of synthesized CeO₂-Mn₂O₃ material is investigated in two environmentally important reactions - ozone decomposition and photocatalytic degradation of Malachite Green dye as model pollutant from aqueous solution under UV irradiation.

As shown in Fig. 6 the ozone conversion degree has been measured in course of 60 minutes. The conversion of ozone was determined using the dependence:

$$O_3 \text{ conversion} = \frac{C_0 - C}{C_0} \times 100\% \quad (2)$$

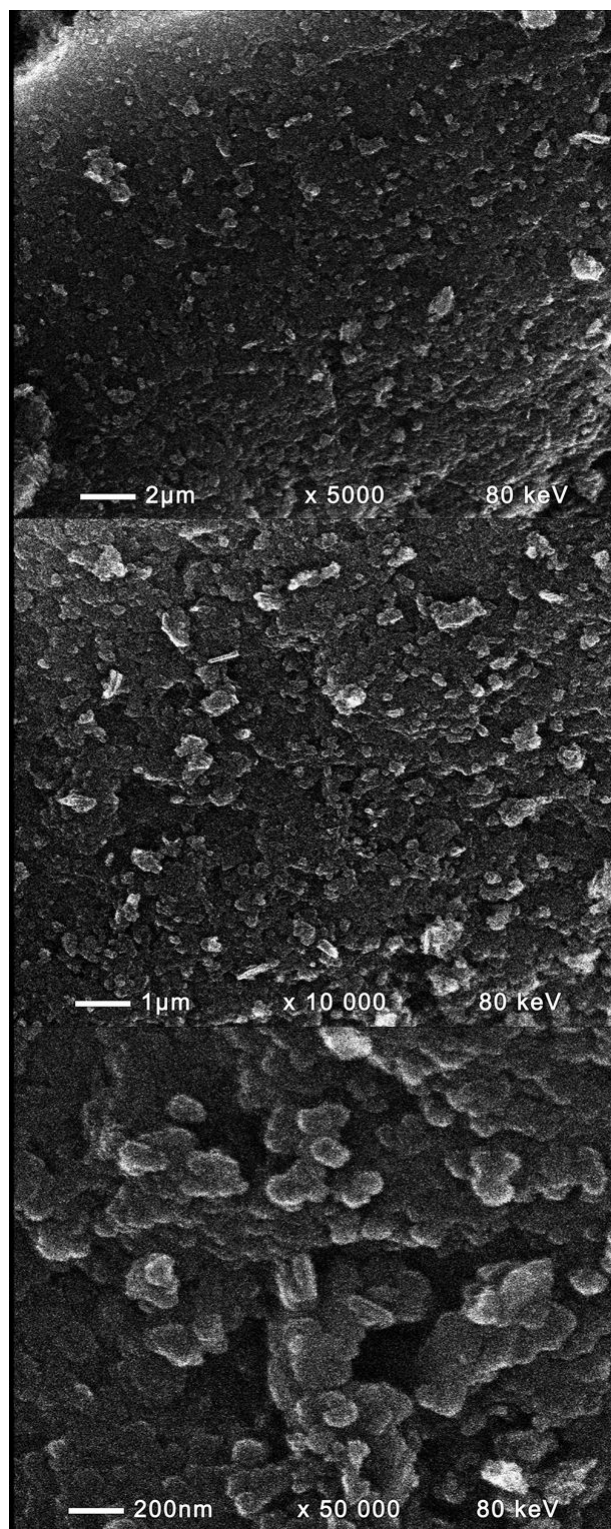


Fig. 5. SEM pictures of $\text{CeO}_2\text{-Mn}_2\text{O}_3$ catalyst at different magnifications: 5000x; 10 000x and 50 000x.

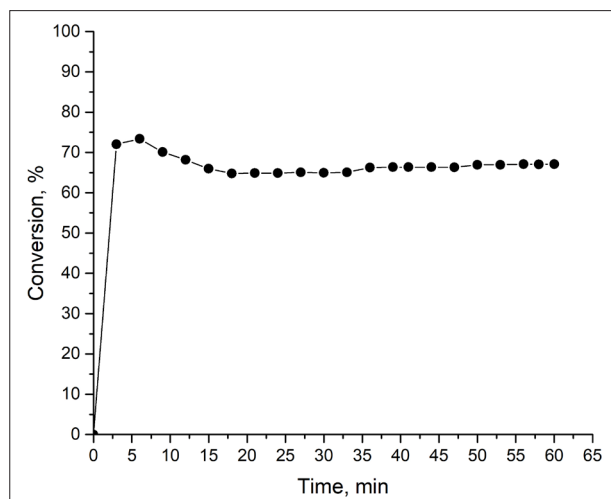


Fig. 6. Ozone conversion reaction over $\text{CeO}_2\text{-Mn}_2\text{O}_3$ catalyst.

where C_0 and C are inlet and outlet concentrations of ozone, respectively.

The conversion degree is almost constant during the time of streaming at room temperature. The obtained ceria-manganese catalyst exhibits high degree of ozone conversion (73 %) at 4 minutes from the start of reaction. The ozone conversion remains high during the all period of the test. It could be supposed that during ozone decomposition on Mn-Ce catalyst occurs formation of intermediate ionic particles possessing either superoxide or peroxide features. It has been reported that the overall ozone decomposition process consists of adsorption of ozone molecule on the surface of catalyst, and then dissociates into an oxygen molecule and an atomic oxygen species. The remaining atomic oxygen species will react with another O_3 molecule to form an adsorbed peroxide species (O_2^{2-}) or superoxide (O_2^-) and an oxygen molecule. The adsorbed O_2^{2-} or O_2^- decompose into oxygen molecules and desorb from the active site of catalysts [39, 40].



The photocatalytic activities of the both non treated and ozonated $\text{CeO}_2\text{-Mn}_2\text{O}_3$ catalysts are presented on Fig. 7. It is illustrating the concentration changes C/C_0

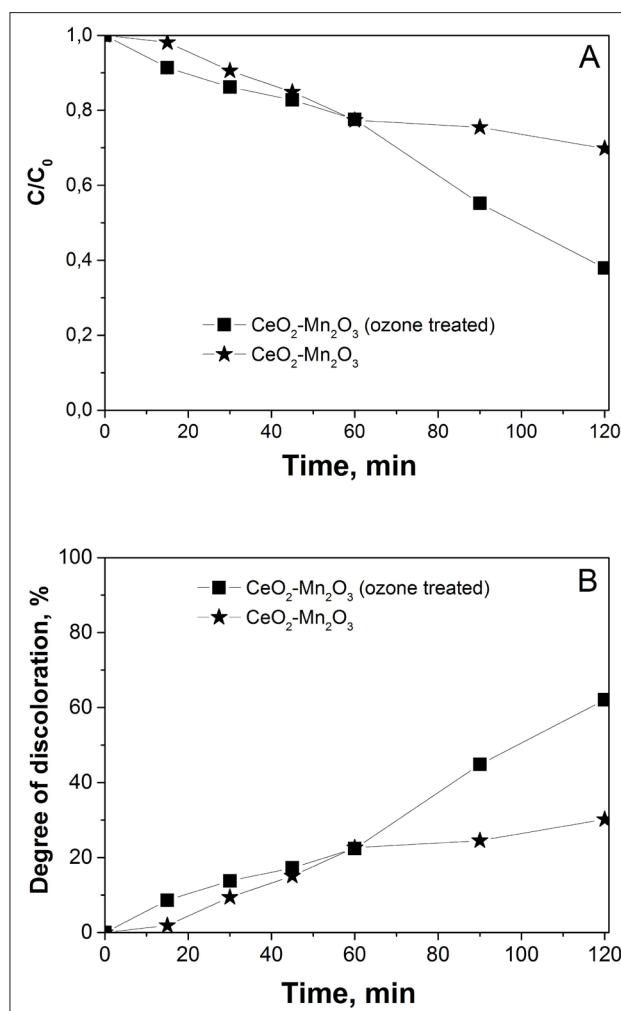
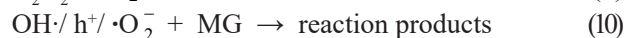
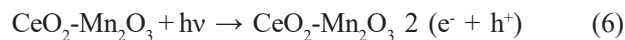


Fig. 7. The concentration ratio C/C_0 (A) and degree of UV discoloration of Malachite Green dye (B). The values C/C_0 were evaluated using the corresponding values of the adsorption peak at 615 nm for MG dye.

and degree of discoloration of MG dye as a function of the UV irradiation time. The degree of dye discoloration was calculated using the dependence: $((C_0 - C)/C_0) \times 100$, where C_0 and C were initial concentration before turning on the illumination and residual concentration of the dye solution after illumination for selected time interval. The ozone treated $\text{CeO}_2\text{-Mn}_2\text{O}_3$ photocatalyst showed the higher degree of discoloration of Malachite Green dye (62 %) compared to that of fresh $\text{CeO}_2\text{-Mn}_2\text{O}_3$ sample (30 %) after 120 minutes illumination.

According to the literature data [22] the degradation mechanism of MG under UV light using $\text{CeO}_2\text{-Mn}_2\text{O}_3$ photocatalyst could be represented by the equations given below:



Ultraviolet light generates excited electrons in the valence band (VB) of the semiconductor oxide material, move to the conduction band (CB) and respectively electron-hole pairs are created in the VB. The holes will react with the surrounding H_2O and generating highly reactive hydroxyl radicals ($\text{OH}\cdot$). Also, highly reactive oxygen radicals ($\cdot\text{O}_2^-$) will be produced when the generated electrons (e^-) react with the surrounding atmospheric oxygen molecules. These reactive species are responsible for MG photodegradation [22].

The adsorption capacities of the investigated $\text{CeO}_2\text{-Mn}_2\text{O}_3$ oxides photocatalysts was estimated using the next formula:

$$Q = \frac{(C_0 - C)V}{m} \quad (11)$$

where C_0 and C are the initial and after 30 minutes in the dark concentrations of the dye, V is the volume of the solution and m is the weight of the samples. The results established that $\text{CeO}_2\text{-Mn}_2\text{O}_3$ oxides photocatalyst used after ozone decomposition demonstrates smaller adsorption capacity (0.0486 mg g^{-1}) in comparison with the fresh photocatalyst (0.0536 mg g^{-1}). It has to note that the higher adsorption capacity of the ozonated photocatalyst does not lead to higher photocatalytic reaction rate. This fact could be due to saturated catalyst active sites with oxygen species during the process of ozone decomposition [41, 42]. According to the investigations of another research group, it could be supposed that the ozone activation modifies the structure of the doped ceria catalysts by formation of surface oxygen vacancies $\text{Ce}^{3+}\text{-V}_{\text{O}_2}$, which induces higher photocatalytic activity and stability [43, 44].

CONCLUSIONS

Pluronic-modified co-precipitation method was applied to obtain high effective mixed $\text{CeO}_2\text{-Mn}_2\text{O}_3$ catalysts towards two environmentally important processes - photocatalytic Malachite Green dye discoloration and ozone decomposition. The obtained mesoporous material possesses toroidal and bottle-

shaped pores. High ozone conversion degree (73 %) was reached during the reaction due to the presence of the active interfaces between CeO₂ and Mn₂O₃ phases. It remains almost constant until to the end of the catalytic tests. The ozone treated CeO₂-Mn₂O₃ catalyst has demonstrated a significantly higher photocatalytic activity towards discoloration of Malachite Green dye (62 %) in comparison with those of the non-treated catalyst (30 %) probably due to the formation of surface oxygen vacancies.

REFERENCES

1. X. Li, J. Ma, H. He, Recent advances in catalytic decomposition of ozone, *J. Environ. Sci.*, 94, 2020, 14-31.
2. Z. Hao, D. Cheng, Y. Guo, Y. Liang, supported gold catalysts used for ozone decomposition and simultaneous elimination of ozone and carbon monoxide at ambient temperature, *Appl. Catal. B: Environ.*, 33, 2001, 217-222.
3. X. Li, J. Ma, H. He, Tuning the chemical state of silver on Ag-Mn catalysts to enhance the ozone decomposition performance, *Environ. Sci. Technol.*, 54, 18, 2020, 11566-11575.
4. T. Batakliiev, V. Georgiev, M. Anachkov, S. Rakovsky, G.E. Zaikov, Ozone decomposition, *Interdiscip. Toxicol.*, 7, 2, 2014, 47-59.
5. J. Ma, C. Wang, H. He, Transition metal doped cryptomelane-type manganese oxide catalysts for ozone decomposition, *Appl. Catal. B: Environ.*, 201, 2017, 503-510.
6. J. Jia, P. Zhang, L. Chen, Catalytic decomposition of gaseous ozone over manganese dioxides with different crystal structures, *Appl. Catal. B: Environ.*, 189, 2016, 210-218.
7. W. Hong, M. Shao, T. Zhu, H. Wang, Y. Sun, F. Shen, X. Li, To promote ozone catalytic decomposition by fabricating manganese vacancies in ε-MnO₂ catalyst via selective dissolution of Mn-Li precursors, *Appl. Catal. B: Environ.*, 274, 2020, 119088.
8. W. Li, S.T. Oyama, Mechanism of ozone decomposition on a manganese oxide catalyst. 2. Steady-state and transient kinetic studies, *J. Am. Chem. Soc.*, 120, 1998, 9047-9052.
9. W.-X. Tang, H.-D. Liu, X.-F. Wu, Y.-F. Chen, Higher oxidation state responsible for ozone decomposition at room temperature over manganese and cobalt oxides: Effect of calcination temperature, *Ozone: Sci. Eng.*, 36, 2014, 502-512.
10. Y. Yu, H. Wang, H. Li, P. Tao, T. Sun, Influence of water molecule on active sites of manganese oxide-based catalysts for ozone decomposition, *Chemosphere*, 298, 2022, 134187.
11. J.-M. Tatibouët, S. Valange, H. Touati, Near-ambient temperature ozone decomposition kinetics on manganese oxide-based catalysts, *Appl. Catal. A: Gen.*, 569, 2019, 126-133.
12. A. Naydenov, R. Stoyanova, D. Mehandjiev, Ozone decomposition and CO oxidation on CeO₂, *J. Mol. Catal. A Chem.*, 98, 1995, 9-14.
13. C.A. Orge, J.J. M. Órfão, M.F.R. Pereira, A.M. Duarte de Farias, M.A. Fraga, Ceria and cerium-based mixed oxides as ozonation catalysts, *Chem. Eng. J.*, 200-202, 2012, 499-505.
14. L. Li, P. Zhang, R. Cao, Porous manganese oxides synthesized with natural products at room temperature: a superior humidity-tolerant catalyst for ozone decomposition, *Catal. Sci. Technol.*, 10, 2020, 2254-2267.
15. I. Spasova, P. Nikolov, D. Mehandjiev, Ozone decomposition over alumina-supported copper, manganese and copper-manganese catalysts, *Ozone: Sci. Eng.*, 29, 1, 2007, 41-45.
16. R. Radhakrishnan, S. Ted Oyama, Ozone decomposition over manganese oxide supported on ZrO₂ and TiO₂: A Kinetic study using in situ Laser Raman Spectroscopy, *J. Catal.*, 199, 2001, 282-290.
17. H. Anwer, A. Mahmood, J. Lee, K.-H. Kim, J.-W. Park, A.C.K. Yip, Photocatalysts for degradation of dyes in industrial effluents: Opportunities and challenges, *Nano Res.*, 12, 2019, 955-972.
18. M.A. Ahmad, R. Alrozi, Removal of malachite green dye from aqueous solution using rambutan peel-based activated carbon: Equilibrium, kinetic and thermodynamic studies, *Chem. Eng. J.*, 171, 2011, 510-516.
19. W.S. Koe, J.W. Lee, W.C. Chong, Y.L. Pang, L.C. Sim, An overview of photocatalytic degradation: photocatalysts, mechanisms, and development of photocatalytic membrane, *Environ. Sci. Pollut. Res.*, 27, 2020, 2522-2565.
20. D. Antony, R. Yadav, Facile fabrication of green nano pure CeO₂ and Mn-decorated CeO₂ with Cassia

- angustifolia seed extract in water refinement by optimal photodegradation kinetics of malachite green, *Environ. Sci. Pollut. Res.*, 28, 2021, 18589-18603.
21. R.A. El-Salamony, W.A. Aboutaleb, Preparation, Characterization of Green Synthesis CeO₂ Nanoparticles and Their Photocatalytic Activity towards Malachite Green Dye, *Chemistry Select*, 7, 9, 2022, e202103722.
 22. I.A. Amar, H.M. Harara, Q.A. Baqul, M.A. Abdul Qadir, F.A. Altohami, M.M. Ahwidi, I.A. Abdalsamed, F.A. Saleh, Photocatalytic degradation of malachite green dye under UV light irradiation using calcium-doped ceria nanoparticles, *Asian J. Nano. Mat.*, 3, 2020, 1-14.
 23. P. Amsaveni, A. Nivetha, C. Sakthivel, C. Suresh Philip, I. Prabha, Effectiveness of surfactants for unique hierarchical Mn₂O₃ nanomaterials as enhanced oxidative catalysts, antibacterial agents, and photocatalysts, *J. Phys. Chem. Solids.*, 144, 2020, 109429.
 24. S. Gnanam, V. Rajendran, Facile hydrothermal synthesis of alpha manganese sesquioxide (α -Mn₂O₃) nanodumb-bells: Structural, magnetic, optical and photocatalytic properties, *J. Alloys Compd.*, 550, 2013, 463-470.
 25. B. Lu, Z. Li, K. Kawamoto, Synthesis of mesoporous ceria without template, *Mater. Res. Bull.*, 48, 2013, 2504-2510.
 26. M.G. Ruiz, J.A. Pliego, L.E.N. Franco, C.M. Álvarez, J.P. Pariente, N.C. Martin Guaregua, Synthesis and characterization of a mesoporous cerium oxide catalyst for the conversion of glycerol, *J. Appl. Res. Technol.*, 16, 6, 2018, 511-523.
 27. B. Deljoo, T. Jafari, R. Miao, M.-P. Nieh, S.L. Suib, M. Aindow, Surfactant selection as a strategy for tailoring the structure and properties of UCT manganese oxides, *Mater. Des.*, 180, 2019, 107902.
 28. W. Kraus, G. Nolze, PowderCell for Windows, Federal Institute for Materials Research and Testing, Berlin, Germany, 2000.
 29. G.K. Williams, W.H. Hall, X-ray line broadening from filed aluminium and wolfram, *Acta Metall.*, 1, 1953, 22-31.
 30. P.M. Shah, L.A. Bailey, S.H. Taylor, The Influence of cerium to manganese ratio and preparation method on the activity of ceria-manganese mixed metal oxide catalysts for VOC total oxidation, *Catalysts*, 13, 2023, 114.
 31. R. Zamiri, H.A. Ahangar, A. Kaushal, A. Zakaria, G. Zamiri, D. Tobaldi, J. M. F. Ferreira, Dielectrical properties of CeO₂ nanoparticles at different temperatures, *PLoS ONE*, 10, 4, 2015, ce0122989.
 32. C. Shao, H. Guan, Y. Liu, X. Li, X. Yang, preparation of Mn₂O₃ and Mn₃O₄ nanofibers via an electrospinning technique, *J. Solid State Chem.*, 177, 2004, 2628-2631.
 33. L. Zhao, Y. Yu, L. Song, M. Ruan, X. Hu, A. Larbot, Preparation of mesoporous titania film using nonionic triblock copolymer as surfactant template, *Appl. Catal. A: Gen.*, 263, 2004, 171-177.
 34. T. Alapi, P. Sipos, I. Ilisz, G. Wittmann, Z. Ambrus, I. Kirisi, K. Mogyorosi, A. Dombi, Synthesis and characterization of titania photocatalysts: the influence of pretreatment on the activity, *Appl. Catal. A: Gen.*, 303, 2006, 1-8.
 35. J. Wang, Q. Liua, A simple method to directly synthesize Al-SBA-15 mesoporous materials with different Al contents, *Solid State Commun.*, 148, 2008, 529-533.
 36. B. Mirtaheri, M. Shokouhimehr, A. Beitollahi, Synthesis of mesoporous tungsten oxide by template-assisted sol-gel method and its photocatalytic degradation activity, *J. Sol-Gel Sci. Technol.*, 82, 2017, 148-156.
 37. D. Skoda, A. Styskalik, Z. Moravec, P. Bezdicka, J. Pinkas, Templated non-hydrolytic synthesis of mesoporous zirconium silicates and their catalytic properties, *J. Mater. Sci.*, 50, 2015, 3371-3382.
 38. L. Truffault, M.-T. Ta, T. Devers, K. Konstantinov, V. Harel, C. Simmonard, C. Andreazza, I.P. Nevirkovets, A. Pineau, O. Veron, J.-P. Blondeau, Application of nanostructured Ca doped CeO₂ for ultraviolet filtration, *Mater. Res. Bull.*, 45, 2010, 527-535.
 39. T. Batakliiev, V. Georgiev, P. Karakashkova, M. Gabrovska, D. Nikolova, M. Anachkov, S. Rakovsky, Gas phase ozone decomposition over co-precipitated Ni-based catalysts, *Bulg. Chem. Commun.*, 49, L, 2017, 24-29.
 40. Y. Liu, P. Zhang, Catalytic decomposition of gaseous ozone over todorokite-type manganese dioxides at room temperature: Effects of cerium modification,

- Appl. Catal. A: Gen., 530, 2017, 102-110.
41. H. Einaga, M. Harada, S. Futamura, Structural changes in alumina-supported manganese oxides during ozone decomposition, *Chem. Phys. Lett.*, 408, 2005, 377-380.
42. R. Radhakrishnan, S. Ted Oyama, Electron transfer effects in ozone decomposition on supported manganese oxide, *J. Phys. Chem. B*, 105, 2001, 4245-4253.
43. M. Zhang, B. Jin, Y. Liu, W. Liu, D. Weng, X. Wu, S. Liu, Ozone activated Ag/CeO₂ catalysts for soot combustion: The surface and structural influences, *Chem. Eng. J.*, 375, 2019, 121961.
44. J. Haber, Fundamentals of hydrocarbon oxidation, *Handbook of Heterogeneous Catalysis: Online*, 2008, pp. 3359.